Multimedia Tools and Applications (2023) 82:12081–12098
https://doi.org/10.1007/s11042-022-13766-3

Bi-SCM: bidirectional spiking cortical model with adaptive unsharp masking for mammography image enhancement

Yaping Yan[1] · Hongjuan Zhang[2] · Songlin Du[3,4,5] · Yide Ma[2]

Received: 8 July 2021 / Revised: 4 August 2022 / Accepted: 1 September 2022 /
Published online: 19 September 2022

Abstract

Mammography technique is commonly used for diagnosing breast cancer, but mammography images usually show low contrast which cause difficulties to clinical diagnosis. Therefore, improving the visual quality of mammography images is an important issue. This is a challenging problem, because every mammography image consists of rich textures, including bright areas, dark areas, and textural details. Inspired by bio-inspired neural network, this paper proposes a Bidirectional Spiking Cortical Model (Bi-SCM) from the perspective of neural information fusion to enhance the contrast of bright areas and dark areas adequately, as well as textural details. This goal is achieved by utilizing the Bi-SCM to first enhance a mammography image and its inverse separately. The enhanced results are fused by a new fusion algorithm based on non-subsampled contourlet transform (NSCT) to ensure that both of the contrast of bright areas and dark areas are adequately improved. The textual details are then enhanced by an unsharp masking method which consists of cubic filter and log-ratio operation. Sufficient experiments on mammography images are conducted to evaluate the proposed approach. Experimental results show that the proposed method outperforms state-of-the-art methods on both enhancing contrast and details. Besides, over-enhancement and noise sensitivity are also significantly suppressed.

Keywords Digital mammography · Image enhancement · Unsharp masking · Bidirectional spiking cortical model (Bi-SCM) · Image fusion

✉ Yaping Yan
yan@seu.edu.cn

[1] School of Computer Science and Engineering, Southeast University, Nanjing 210096, China

[2] School of Information Science and Engineering, Lanzhou University, Lanzhou 730000, China

[3] School of Automation, Southeast University, Nanjing 210096, China

[4] Hubei Key Laboratory of Advanced Control and Intelligent Automation for Complex Systems, Wuhan 430074, China

[5] Engineering Research Center of Intelligent Geodetection Technology, Ministry of Education, Wuhan 430074, China

1 Introduction

Breast cancer is one of the most common diseases and the leading cause of death among women. Although it is hard to prevent the development of breast cancer, early detection of tumors can significantly improve clinical cure rates [39]. There exists several imaging techniques for breast exam, among which mammography (X-ray image) is the most common technique for radiologists to detect and diagnose breast cancer [16]. If the mammography images are noised during imaging or transmitting [5], they can be recovered by some denoising methods [7–9]. But more seriously, mammography images are usually limited by X-ray hardware systems and exhibit poor resolution and low contrast. Different from denoising, effective enhancement approaches are desired to solve the problems of poor resolution and low contrast. To this end, several enhancement algorithms have been proposed, such as the multiscale representation [14, 20, 23], histogram equalization (HE) [3, 4, 17, 21, 22], and unsharp masking (UM) [26, 27, 35, 36, 45].

1.1 Related works

Multiscale decomposition has been frequently employed in mammogram enhancement. The main idea is to perform a multiscale computation framework, such as discrete wavelet transform (DWT) [20], curvelet transform [14], or contourlet transform [23], on mammograms followed by the modification of the transform coefficients in each subband of the multiscale representation. Finally, performing the corresponding inverse transform on the modified coefficients to get the enhanced mammograms. Besides enhancement, multiscale decomposition is also widely used for medical images denoising. Manoj Diwakar et al. [6, 10, 11] studied this problem deeply and proposed a variety of multiscale decomposition based medical images denoising methods. However, it is argued that multiscale representation cannot efficiently show edges and textured region in images [24].

Histogram equalization, which is known for its simpleness and the ability of improving contrast, is a desirable technique for image enhancement. But conventional HE algorithms may cause over-enhancement and the intensity saturation effects. So many improved algorithms, such as the brightness-preservation HE algorithm [4, 22], histogram partitioning method [3], and texture enhanced HE approach [17] have been proposed. Although the brightness-preservation HE algorithm maintains a natural look and reduces saturation effect in the output image, it also generates annoying side effects depending on the variation in the gray-level distribution [17]. The histogram partitioning algorithm divides an image histogram into several subintervals and modifies each subinterval separately. However, pixels with the similar intensity may belong to different intervals, producing over-enhancement in some image regions [21]. The texture enhanced HE approach was proposed to avoid the occurrence of over-enhancement and the intensity saturation effects, but the degree of contrast enhancement is not significant.

Several algorithms have been developed for mammography image enhancement by using unsharp masking. The traditional UM method is sensitive to noise and may generate ringing artifacts. To rectify these limitations, various modified approaches have been suggested, such as the rational UM (RUM) [36], cubic UM (CUM) [35], adaptive UM (AUM) [26], HE based UM [45], and nonlinear UM (NUM) [27]. These algorithms attempt to enhance image details, but usually result in different degrees of over-enhancement. Besides, they are powerless in improving image contrast.

1.2 Contributions

Micro-calcifications and masses are the main abnormalities in mammography images, which are important basis for the diagnosis of breast cancer. Micro-calcifications are tiny calcium deposits in breast tissue. They appear in images as bright, 100-um dots or clusters of dots, which are difficult to detect. Breast masses are bright spots on the image. Most of the masses have blurred boundaries and low contrast, which are easy to be confused with the normal tissues of the breast. Because of the limitations of X-ray hardware systems, the hypothesis of this paper is that the visual quality of mammography images is low because of poor resolution and low contrast. In order to overcome the problems in the detection of micro-calcifications and masses, this paper proposes a bidirectional spiking cortical (Bi-SCM) method to improve contrast as well as enhance details of mammography images. The goal of this paper is to highlight the lesion area without losing image details and introducing background noise, so as to assist doctors in diagnosis and provide technical support for computer aided mammography detection system. The main contributions of this paper can be briefly summarized as follows.

1. A Bi-SCM framework is proposed from the perspective of neural information fusion to enhance the contrast of bright areas and dark areas adequately, as well as textural details.
2. Based on the proposed Bi-SCM framework, neural spiking model is utilized to enhance a mammography image and its inverse, and then a NSCT based fusion method is proposed to fuse the primarily enhanced results, ensuring both contrasts of bright areas and dark areas are adequately improved.
3. We made the first attempt to further enhance the textual details of the NSCT-fused mammography image with an adaptive unsharp masking method which consists of cubic filter and log-ratio operation.
4. Sufficient experiments on real mammography images are conducted to prove that the proposed method outperforms state-of-the-art methods on both enhancing contrast and details.

The novelties of the proposed method are as follows. First, Bi-SCM framework is proposed from the perspective of neural information fusion to enhance mammography images. By taking into account both intensity distribution and spatial structure information, Bi-SCM can enhance lesions while suppressing background noises. Secondly, an original fusion rule, named weighted region energy, is proposed to fuse the two SCM-enhanced results while avoiding information loss. By using the directive contrast as weighting factor, more details in mammograms can be preserved. The rest of this paper is organized as follows. Section 2 presents the framework and details of the proposed Bi-SCM method. Experimental results on real mammography images are reported and analyzed in Section 3, followed by Section 4 which gives a overall conclusion of the paper.

2 Methodology

2.1 Bidirectional spiking cortical model

In the late 1980s, Eckhorn et al. [13] studied the mechanism of cat visual cortex, and found that the binary images produced by the midbrain in an oscillating manner are distinctive representations of visual features. Based on this discovery, a a feedback neural network model

entitled pulse coupled neural network (PCNN) [37], which consists of a feedback field, a modulation field and a pulse generation field was proposed. In our previous work [47], a modified version of pulse coupled neural network (PCNN) model entitled spiking cortical model (SCM), was proposed for invariant texture retrieval. The SCM is mathematically described by

$$U_{ij}[n] = fU_{ij}[n-1] + S_{ij}\sum_{kl} W_{ijkl}Y_{kl}[n-1] + S_{ij}, \tag{1}$$

$$E_{ij}[n] = gE_{ij}[n-1] + hY_{ij}[n-1], \tag{2}$$

$$Y_{ij}[n] = \begin{cases} 1, & U_{ij}[n] > E_{ij}[n] \\ 0, & \text{otherwise} \end{cases}, \tag{3}$$

where n denotes iteration times, and N_{ij} denotes the neuron in the position (i, j). Neuron N_{ij} has internal activity $U_{ij}[n]$ and dynamic threshold $E_{ij}[n]$, which retain the previous states by decay factors f and g, respectively. W is the synaptic weight, denoting influence of neighboring neurons, S_{ij} denotes input stimulus, and Y_{ij} is the output of neuron N_{ij}. Internal activity $U_{ij}[n]$ is compared with the dynamic threshold $E_{ij}[n]$ to judge whether neuron N_{ij} fires ($Y_{ij}[n] = 1$) or not ($Y_{ij}[n] = 0$). Subsequently, if neuron N_{ij} fires, the dynamic threshold would increase by amplitude h suddenly, otherwise the dynamic threshold would decay by a factor g. In addition, $Y_{kl}[n-1]$ denotes the output of neighboring neuron in the previous iteration.

Although SCM can enhance low contrast images, it processes contrast varying with intensities. When SCM is used to enhance images, bright areas would be processed more coarsely than dark areas [47]. It is therefore not suitable for mammogram enhancement, because both bright and dark areas provide important information in mammograms. In this paper, we proposes an improved the Bi-SCM model to overcome this problem. A graphical illustration of our approach is shown in Fig. 1. The original mammography image $I(i, j)$ is firstly fed into a cubic filter to obtain the textual details $z(i, j)$ and the corresponding smoothed version $S(i, j)$. Then a bi-directional SCM model is proposed to enhance the

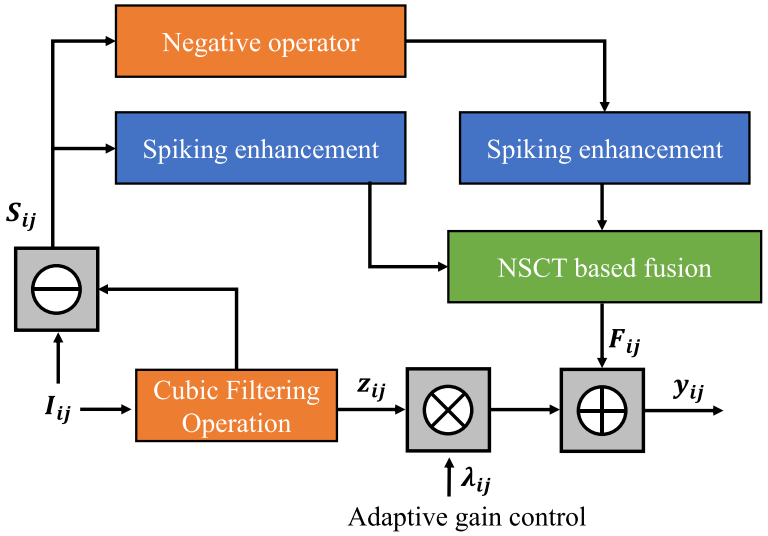

Fig. 1 Framework of the proposed Bi-SCM

smoothed image. The two SCM-enhanced results are further fused as a single out, which leads to anomalies being highlighted while the background textures and noises are suppressed. The final enhancement result is obtained by adding the detailed image to the fused image with adaptive gain control. The main motivation is to adequately enhance both of the bright areas and dark areas. For both original mammogram and the corresponding reverse mammogram, before a neuron pulses for the first time, it has no linking input, so its internal activity can be derived from (1) and described as

$$\begin{aligned} U_{ij}[n] &= fU_{ij}[n-1] + S_{ij} \\ &= (U_{ij}[0] - \frac{S_{ij}}{1-f}) f^n + \frac{S_{ij}}{1-f}. \end{aligned} \tag{4}$$

Its dynamic threshold E_{ij} can be derived from (2) and expressed by

$$E_{ij}[n] = gE_{ij}[n-1] = g^n E_{ij}[0]. \tag{5}$$

When $U_{ij}[n] = E_{ij}[n]$, the neuron N_{ij} fires for the first time. Therefore, the first iteration times can be given by

$$n_{1ij} = -\frac{1}{\ln g} \ln \frac{E_{ij}[0]}{U_{ij}[n_{1ij}]}. \tag{6}$$

Since time matrix is defined to record the first iteration times for all neurons, if the internal activity U_{ij} is equal to its stimulus S_{ij}, the time matrix of SCM can be approximated as

$$T_{ij} = n_{1ij} = -\frac{1}{\ln g} \ln \frac{E_{ij}[0]}{U_{ij}[n_{1ij}]} \approx -\frac{1}{\ln g} \ln \frac{E_{ij}[0]}{S_{ij}}. \tag{7}$$

and thus

$$\ln S = T \ln g + \ln E[0]. \tag{8}$$

On the other hand, Weber-Fechner law is described by [15]

$$I = k \ln S + r, \tag{9}$$

where I is the human visual perception, S is the stimulus at the instant, k is a constant factor which is to be determined experimentally, and r is the constant of integration. Substituting (8) into (9), one achieve

$$I = k(T \ln g + \ln E[0]) + r = -k'T + r', \tag{10}$$

where $k' = k/\ln g$, and $r' = k \ln E[0] + r$. Equation (10) describes the link between the subjective sense of intensity I and the time matrix T, where I can be obtained by computing the negative time matrix. Therefore, the negative time matrix of SCM conforms to Weber-Fechner law, and can be directly regarded as the enhanced result. The internal activity is initialized to 0, i.e., $U_{ij}[0] = 0$. Thus, equation (4) can be rewritten as

$$U[n_1] = -\frac{S}{1-f} f^{n_1} + \frac{S}{1-f} = \frac{1-f^{n_1}}{1-f} S. \tag{11}$$

Substituting (11) into (7), we achieve

$$T = -\frac{1}{\ln g} \ln \left(\frac{1-f}{1-f^{n_1}} \cdot \frac{E[0]}{S} \right). \tag{12}$$

In addition, according to the lateral inhibition principle of the human visual system (HVS), Laplacian of Gaussian (LoG) operator can be used for image edge sharpening, and the initial value of dynamic threshold can be obtained as [25]

$$E[0] = 1 + S \otimes \mathrm{LoG}. \tag{13}$$

Therefore, as can be seen from (12) and (13), values of time matrix only depend on input stimulus and decay factors f and g, where $0 < f < g < 1$. To insure changes in E and U occur slowly, the value of f is close to 0, and the value of g is just under 1.

To fuse the enhanced images of original mammogram and the corresponding reverse mammogram, we propose to use the multi-scale and multi-directional computation framework entitled NSCT, which consists of a nonsubsampled pyramid Laplacian filter and a nonsubsampled directional filter [2]. Comparing with wavelet transform and contourlet transform, NSCT shows better translational invariance and makes full use of the geometric regularity in images, so that it has better multidirectional selectivity and provides more detailed information. Thereby, NSCT is a desirable technique for this purpose. The NSCT based image fusion methods usually consist of three steps. Firstly, the source mammograms are transformed by NSCT to obtain low- and high-frequency components. Then two different fusion rules are used to fuse low- and high-frequency coefficients, respectively. Finally, the fused image is constructed by the inverse NSCT with all fused subimages. More detailed discussion can be found in [2]. In this subsection, we introduce a modified NSCT based fusion method to fuse the SCM enhanced mammogram and its enhanced reverse version. Weighted region energy and directive contrast are selected as the fusion rules of low- and high-frequency coefficients, respectively. The proposed fusion framework can preserve more details in source mammograms and further improve the quality of fused mammogram.

HVS is sensitive to intensity contrast, but insensitive to luminance value at independent positions. Therefore, it is necessary to quantify the intensity contrast. The local luminance contrast is defined as [42]

$$R = \frac{L - L_B}{L_B}, \tag{14}$$

where L denotes the luminance at a certain location in the image plane, and L_B represents the luminance of the local background, regarded as low frequency component. Hence, $L - L_B$ can be taken as local high-frequency component. The local luminance contrast can be further extended as directive contrast in multiscale domain, which is given by [2]

$$D_{l,\theta}(i,j) = \begin{cases} \left(\frac{1}{C_\ell(i,j)}\right)^{\partial} \frac{SML_{l,\theta}(i,j)}{C_\ell(i,j)}, & if\ C_\ell(i,j) \neq 0 \\ SML_{l,\theta}(i,j), & if\ C_\ell(i,j) = 0 \end{cases}, \tag{15}$$

where $C_\ell(i,j)$ is the low-frequency subband at the coarsest level ℓ, ∂ is a visual constant representing the slope of the best fitted lines through high-contrast data, and $SML_{l,\theta}(i,j)$ is the sum-modified-Laplacian of the NSCT high-frequency subband at scale l and orientation θ, which is computed over a $(2P+1) \times (2Q+1)$ pixel block, given by

$$SML_{l,\theta}(i,j) = \sum_{m=i-P}^{i+P} \sum_{n=j-Q}^{j+Q} \nabla^2_{l,\theta} H(m,n), \tag{16}$$

and

$$\begin{aligned} \nabla^2_{l,\theta} H(i,j) = & \left|2H_{l,\theta}(i,j) - H_{l,\theta}(i-1,j) - H_{l,\theta}(i+1,j)\right| \\ & + \left|2H_{l,\theta}(i,j) - H_{l,\theta}(i,j-1) - H_{l,\theta}(i,j+1)\right|, \end{aligned} \tag{17}$$

where $H_{l,\theta}(i,j)$ is the high-frequency subband at position (i,j), scale l, and orientation θ. It has been proved that the directive contrast is less sensitive to noise and provides the most salient features [2]. Therefore, in order to select the most prominent texture and edge information, we use the directive contrast to fuse high-frequency coefficients.

Region energy is computed over a $(2M+1)\times(2N+1)$ (usually 3×3, 5×5, or 7×7) pixel block as [44]

$$RE(i,j)=\sum_{m=-M}^{M}\sum_{n=-N}^{N}\left(I\left(i+m,j+n\right)-I\left(i,j\right)\right)^2, \tag{18}$$

where $I(i,j)$ represents the gray value at position (i,j). In general, pixels with larger values of region energy represent the salient features of the image, such as edges and lines. So we can regard region energy as a quantitative metric of image clarity and use it to fuse low-frequency subimages. The fused low-frequency is calculated by

$$C_\ell^F\left(i,j\right)=\begin{cases} C_\ell^A\left(i,j\right), & RE_{C_\ell^A}\left(i,j\right)\geq RE_{C_\ell^B}\left(i,j\right)\\ C_\ell^B\left(i,j\right), & RE_{C_\ell^A}\left(i,j\right)< RE_{C_\ell^B}\left(i,j\right)\end{cases}, \tag{19}$$

where A and B are two input images. C_ℓ^A and C_ℓ^B denote low-frequency subbands at the coarsest level of A and B, respectively. Region energy based fusion rule can extract more details, and is less sensitive to noises [44]. However, when the region energies of two corresponding pixels are close to each other, this method may lead to information loss. Therefore, we propose a novel fusion criterion based on weighted region energy. The weighted region energy of the low-frequency subband at the coarsest level is defined as

$$WE_\ell(i,j)=D_\ell\left(i,j\right)\cdot RE\left(i,j\right), \tag{20}$$

where $D_\ell(i,j)$ denotes the directive contrast in NSCT domain. When the difference between the region energies of two corresponding pixels is great, the NSCT coefficients with larger region energy are selected as fused coefficients. On the other hand, when the region energies of two corresponding pixels are close to each other, the fused low-frequency is calculated by

$$C_\ell^F\left(i,j\right)=\frac{\left(WE_\ell^A\left(i,j\right)C_\ell^A\left(i,j\right)+WE_\ell^B\left(i,j\right)C_\ell^B\left(i,j\right)\right)}{\left(WE_\ell^A\left(i,j\right)+WE_\ell^B\left(i,j\right)\right)}, \tag{21}$$

Since directive contrast $D_l(i,j)$ is the extension of local luminance contrast in multi-resolution domain, from (20) and (21), we can find that more information will be extracted from pixels with larger local contrast. Thus, by classing the fusion task into two cases and use the directive contrast as weighting factor, the proposed fusion rule is able to avoid information loss while improve the contrast of fused mammograms.

The proposed image fusion scheme includes the following steps:

- **NSCT Based Decomposition**
  Perform ℓ-level NSCT on the source images A and B to obtain their low-frequency subimages C_ℓ^A, C_ℓ^B and a series of high-frequency subimages $H_{l,\theta}^A$, $H_{l,\theta}^B$ at each level $l\in[1,\ \ell]$ and direction θ, i.e., A : $\left\{C_\ell^A, H_{l,\theta}^A\right\}$ and B : $\left\{C_\ell^B, H_{l,\theta}^B\right\}$.
- **Fusion of High-frequency Subimages**
  The high-frequency coefficients usually include most details and edge features of the source image. Since directive contrast can be thought as an quantitative expression of image detail and be less sensitive to noise, we select directive contrast as the fusion rule for high-frequency subimages. Firstly, the directive contrast for NSCT high-frequency subimages is computed using (15)-(17), denoted by $D_{H_{l,\theta}^A}$ and $D_{H_{l,\theta}^B}$ at each level l in direction θ, respectively. Then the high-frequency coefficients are fused, and the fused

high-frequency coefficients $H_{l,\theta}^{F}$ are defined by

$$H_{l,\theta}^{F}(i,j) = \begin{cases} H_{l,\theta}^{A}(i,j), & D_{H_{l,\theta}^{A}}(i,j) \geq D_{H_{l,\theta}^{B}}(i,j) \\ H_{l,\theta}^{B}(i,j), & D_{H_{l,\theta}^{A}}(i,j) < D_{H_{l,\theta}^{B}}(i,j) \end{cases} \tag{22}$$

– **Fusion of Low-frequency Subimages**

The low-frequency coefficients usually represent the approximation component of the source images. The simplest way to get the fused bands is conventional averaging [2]. However, it leads to information loss and low contrast of the fused image. Selecting low-frequency coefficients is still an open problem. In this subsection, we propose a novel fusion rule based on weighted region energy for low-frequency subimages. Firstly, the region energy and the weighted region energy for NSCT low-frequency subimages are computed with (18) and (20), denoted by $RE_{C_\ell^A}$, $RE_{C_\ell^B}$, $WE_{C_\ell^A}$ and $WE_{C_\ell^B}$, respectively. Then we choose fusion rule by estimating the difference between the region energies of two corresponding pixels. If the region energies of two corresponding pixels are close to each other, i.e., $\left|RE_{C_\ell^A} - RE_{C_\ell^B}\right| > T$, where T is a threshold which is normally set as 0.1, the fused low-frequency is calculated by (19). If $\left|RE_{C_\ell^A} - RE_{C_\ell^B}\right| \leq T$, the fused low-frequency coefficients C_ℓ^F is calculated by (21).

– **Inverse NSCT Based Reconstruction**

Perform ℓ-level inverse NSCT on the fused low-frequency $\left(C_\ell^F\right)$ and high-frequency $\left(H_{l,\theta}^{F}\right)$ subimages to get the fused image F.

2.2 Adaptive unsharp masking

Besides contrast that can be well enhanced by the proposed Bi-SCM, textual details are also very important for mammography images. In conventional enhancement models, unsharp masking [26] is usually adopted for enhancing textual details. In particular, every pixel $y(i,j)$ in the enhanced image can be obtained from original image I through

$$y(i,j) = I(i,j) + \lambda\, z(i,j), \tag{23}$$

where $z(i,j)$ is a high-passed version of the input image, and λ is the enhancement factor. The traditional UM can enhance details in the original image effectively. However, using a universal enhancement gain for the whole image leads to over-enhancement and noise amplification. In this paper, to suppress the noise sensitivity, a cubic filter [35] is employed to acquire $z(i,j)$, which is defined as

$$\begin{aligned} z(i,j) = &\left(I_{i-1,j} - I_{i+1,j}\right)^2 \left(2I_{i,j} - I_{i-1,j} - I_{i+1,j}\right) \\ &+ \left(I_{i,j-1} - I_{i,j+1}\right)^2 \left(2I_{i,j} - I_{i,j-1} - I_{i,j+1}\right). \end{aligned} \tag{24}$$

On the other hand, in order to reduce the over-enhancement, we choose the log-ratio operations and adaptive gain control algorithm [12] instead of arithmetic operations and universal enhancement gain, respectively. The output of the adaptive UM scheme becomes

$$y(i,j) = I \oplus [\lambda(z) \otimes z], \tag{25}$$

$$\lambda(z) = \partial + \beta \exp(-|2z-1|^{\gamma}), \tag{26}$$

where γ is a decreasing factor, and $\gamma > 0$. The addition operation $\oplus$ and scalar multiplication operation $\otimes$ of the log-ratio operations are formally defined as

$$\psi(x) = \frac{1-x}{x}, \tag{27}$$

$$x_1 \oplus x_2 = \frac{1}{1 + \psi(x_1)\,\psi(x_2)}, \tag{28}$$

$$\lambda \otimes x = \frac{1}{1 + \psi(x)^{\lambda}}. \tag{29}$$

The gray scale set is closed under log-ratio operations. In order to avoid over-enhancement, λ is excepted to gradually decrease from $\lambda_{\max}$ when the value of z is moderate to $\lambda_{\min}$ when z is high or low. Thus, we can assume $\lambda_{\max} = \lambda(1)$ and $\lambda_{\min} = \lambda(0.5)$. Then the two parameters ∂ and β can be obtained by

$$\beta = (\lambda_{\max} - \lambda_{\min}) / \left(1 - e^{-1}\right) \tag{30}$$

and

$$\partial = \lambda_{\max} - \beta, \tag{31}$$

respectively. The proposed adaptive UM algorithm can significantly enhance details while avoid over-enhancement. The values of parameters γ, $\lambda_{\max}$, and $\lambda_{\min}$ depend on the contrast of the input mammogram. We experimentally found that the choices of $\gamma = 0.005$, $\lambda_{\max} = 3$, and $\lambda_{\min} = 1$ are effective in providing good results to almost all tested mammograms.

3 Experimental results and discussions

This section provides the experimental results and a comprehensive discussion of the proposed approach. Mammograms for experiments are from the mini-mammographic image analysis society (MIAS) database of mammograms [40] and the digital database for screening mammography (DDSM) of the University of South Florida [19]. All test mammograms are cropped into images with smaller size which contain masses, micro-calcifications or abnormal regions.

3.1 Comparison of fusion methods

To evaluate the proposed fusion method, it was tested on 100 mammograms, half of which come from the MIAS database and others come from the DDSM database. Sufficient state-of-the-art approaches are taken into comparison, including PCNN [43], wavelet [31], contourlet [33], and NSCT (NSCT-1 [2] and NSCT-2 [41]) based methods. For wavelet, contourlet, and NSCT based methods, the level of decomposition is set to 3, and wavelet based method uses the 'db4' wavelet as basis. Typical fusion results are visualized in Fig. 2.

Mutual information (MI) and edge based similarity measure $Q^{AB/F}$ are commonly used objective criteria for evaluation of fusion algorithms [28]. Specifically, MI is utilized to measure the mutual dependence of the fused image F and two input images A and B. In other words, MI reflects how much information of the original image is obtained by the fused image, which is expressed as [32]

$$MI = MI(A, F) + MI(B, F), \tag{32}$$

and

$$MI(U, V) = \sum_{u \in U} \sum_{v \in V} p(u, v) \log_2 \frac{p(u, v)}{p(u)\,p(v)}, \tag{33}$$

where $p(u, v)$ is the joint probability distribution function of U and V, and $p(u)$ and $p(v)$, which are the marginal probability distribution functions of U and V, respectively, can be obtained by simple normalization of the joint and marginal histograms of both variables.

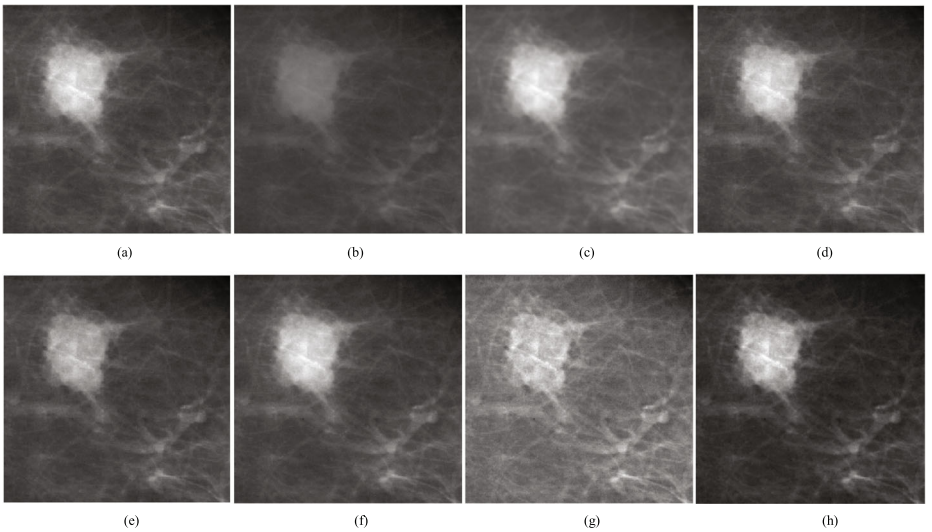

Fig. 2 Comparison of mammogram fusion results with different fusion algorithms. (a) Enhanced mammogram from conventional SCM; (b) Enhanced reverse mammogram from conventional SCM;(c) Fused results by PCNN; (d) Contourlet; (e) Wavelet; (f) NSCT-1; (g) NSCT-2; (h) The proposed fusion method

On the other hand, ESM computes the similarity of edges between the fused image and input images, which measures the ability of the fusion process to transfer important detail information as accurately as possible, and is given by [46]

$$Q^{AB/F} = \frac{\sum_{i=1}^{M}\sum_{j=1}^{N}\left[Q_{i,j}^{AF} w_{i,j}^{A} + Q_{i,j}^{BF} w_{i,j}^{B}\right]}{\sum_{i=1}^{M}\sum_{j=1}^{N}\left[w_{i,j}^{A} + w_{i,j}^{B}\right]}, \tag{34}$$

where $w_{i,j}^{A}$ and $w_{i,j}^{B}$ are the weighting coefficients. $Q_{i,j}^{AF}$ and $Q_{i,j}^{BF}$ are defined as

$$Q_{i,j}^{AF} = Q_{g}^{AF}(i,j)\, Q_{\alpha}^{AF}(i,j) \tag{35}$$

and

$$Q_{i,j}^{BF} = Q_{g}^{BF}(i,j)\, Q_{\alpha}^{BF}(i,j), \tag{36}$$

where Q_{g}^{*F} and Q_{α}^{*F} are the edge strength and orientation preservation values at location (i, j), respectively, and can be derived

$$Q_{g}^{*F}(i,j) = \frac{\Gamma_g}{1 + e^{\kappa_g (G^{*F}(i,j) - \sigma_g)}} \tag{37}$$

and

$$Q_{\alpha}^{*F}(i,j) = \frac{\Gamma_\alpha}{1 + e^{\kappa_\alpha (\Delta^{*F}(i,j) - \sigma_\alpha)}}, \tag{38}$$

where the constants Γ_*, κ_*, and σ_* determine the shape of the sigmoid functions used to form the edge strength and orientation preservation value. G^{*F} and Δ^{*F}, which represent the relative strength and orientation values between input image and fused image

respectively, are given by

$$G^{*F}(i,j) = \begin{cases} \frac{g_F(i,j)}{g_*(i,j)}, & g_*(i,j) > g_F(i,j) \\ \frac{g_*(i,j)}{g_F(i,j)}, & \text{otherwise} \end{cases} \tag{39}$$

and

$$\Delta^{*F}(i,j) = 1 - \frac{|\alpha_*(i,j) - \alpha_F(i,j)|}{\pi/2}. \tag{40}$$

The edge strength g_* and orientation α_* are got by a Sobel edge operator, i.e.

$$g_*(i,j) = \sqrt{s_*^x(i,j)^2 + s_*^y(i,j)^2} \tag{41}$$

$$\alpha_*(i,j) = \tan^{-1}\left(\frac{s_*^x(i,j)}{s_*^y(i,j)}\right), \tag{42}$$

where s_*^x and s_*^y are the convolved results with the horizontal and vertical Sobel templates.

Table 1 reports the average MI values and average $Q^{AB/F}$ values of each database for all tested mammograms. All two fusion scores are normalized where values closer to 1 indicate a higher quality of the fused image. And the best records are marked in bold. From Fig. 2 and Table 1, we can see that PCNN cannot capture features at different levels and bandwidths, as shown in Fig. 2(c). This problem is overcome in multi-resolution based algorithms, especially NSCT based algorithms. This result is from the fact that NSCT can provide better shift invariance and multidirectional selectivity than other multiscale analysis tools. Among NSCT based algorithms, the proposed method performs best. The algorithm in [41] uses local entropy and region energy to fuse low- and high-frequency coefficients respectively, leading to low contrast of the fused image, as shown in Fig. 2(f). The performances of the algorithm in [2] and the proposed method are close to each other, giving better results compared to others algorithms, as shown in Fig. 2(g) and (h), respectively. However, looking carefully at the results, the proposed algorithm not only improves the visual effect of the fused image, but also preserves more details in the source image. This is due to the fact that our method can reduce the information loss and improve the contrast of the fused images. In conclusion, both subjective and objective evaluations prove the superiority of the proposed algorithm.

3.2 Comparison of enhancement performance

The proposed enhancement method is tested on 50 mammograms obtained from the MIAS database, and compared with several well-known enhancement algorithms, including the RUM [36], nonseparable cubic UM (NSCUM) [35], generalized UM (GUM) [12], AUM [30], multi-scale retinex (MSR) [34], and brightness preserving dynamic fuzzy HE (BPDFHE) [38]. Typical mammograms and the corresponding enhanced results are shown in Figs. 3, 4, 5 and 6. The initial values of the parameters are listed in Table 2.

Table 1 Average evaluation indices for fused mammograms

Database	Criteria	PCNN	wavelet	Contourlet	NSCT-1	NSCT-2	Bi-SCM
MIAS	MI	0.5689	0.7741	0.6058	0.7714	0.4583	**0.8336**
	$Q^{AB/ABF}$	0.5345	0.7972	0.8030	0.8107	0.7646	**0.8196**
DDSM	MI	0.6642	0.8425	0.6959	0.8768	0.5581	**0.9181**
	Q^{ABABF}	0.5326	0.7769	0.7773	0.7928	0.6983	**0.7943**

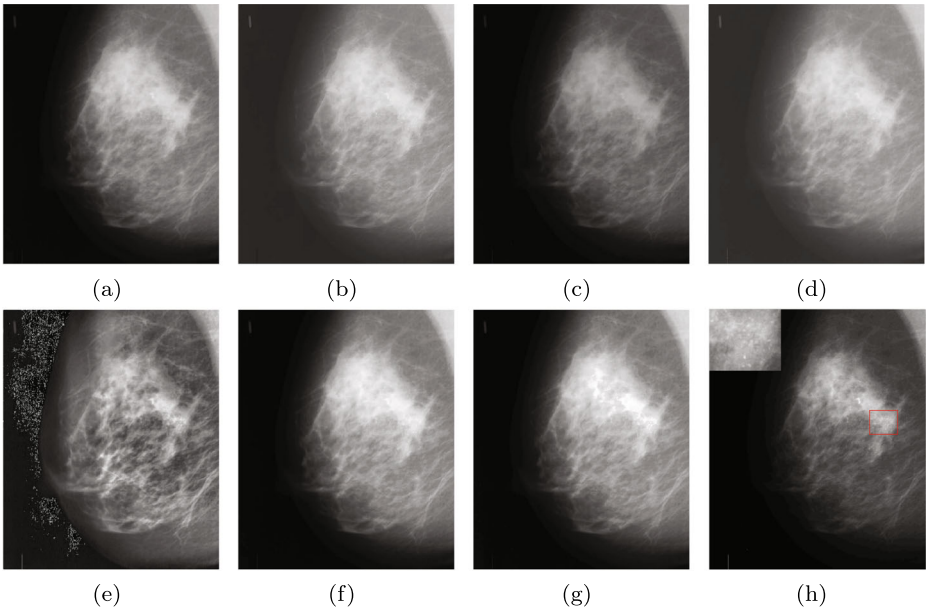

Fig. 3 Comparison of mammogram enhancement with different algorithms. (a) Original mammogram. Enhanced results by (b) RUM; (c) NSCUM; (d) AUM; (e) GUM; (f) MSR; (g) BPDFHE; (h) The proposed Bi-SCM. Note that RUM, NSCUM, AUM, and GUM are UM based methods; MSR is MD based method; BPDFHE is HE based method

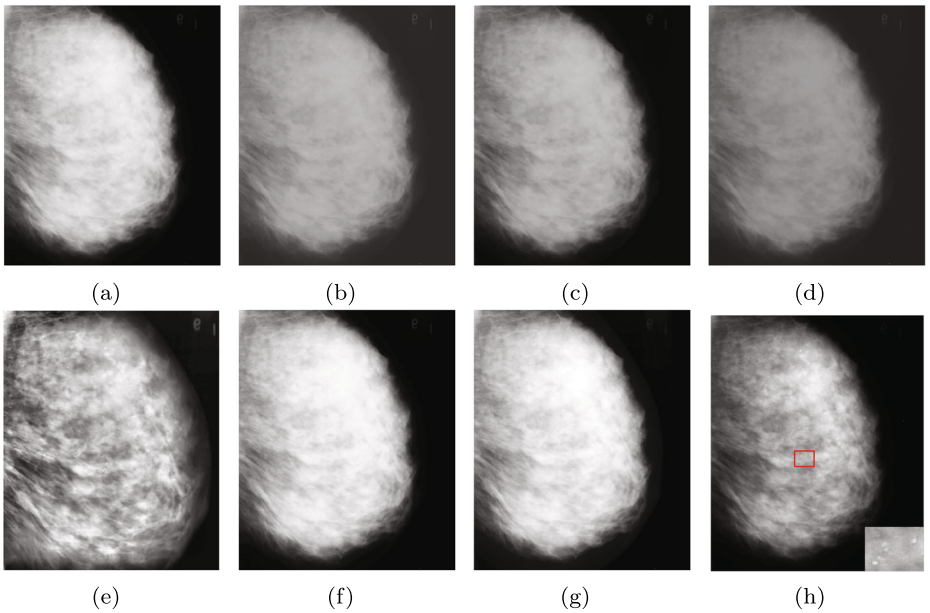

Fig. 4 Comparison of mammogram enhancement with different algorithms. (a) Original mammogram. Enhanced results by (b) RUM; (c) NSCUM; (d) AUM; (e) GUM; (f) MSR; (g) BPDFHE; (h) The proposed Bi-SCM. Note that RUM, NSCUM, AUM, and GUM are UM based methods; MSR is MD based method; BPDFHE is HE based method

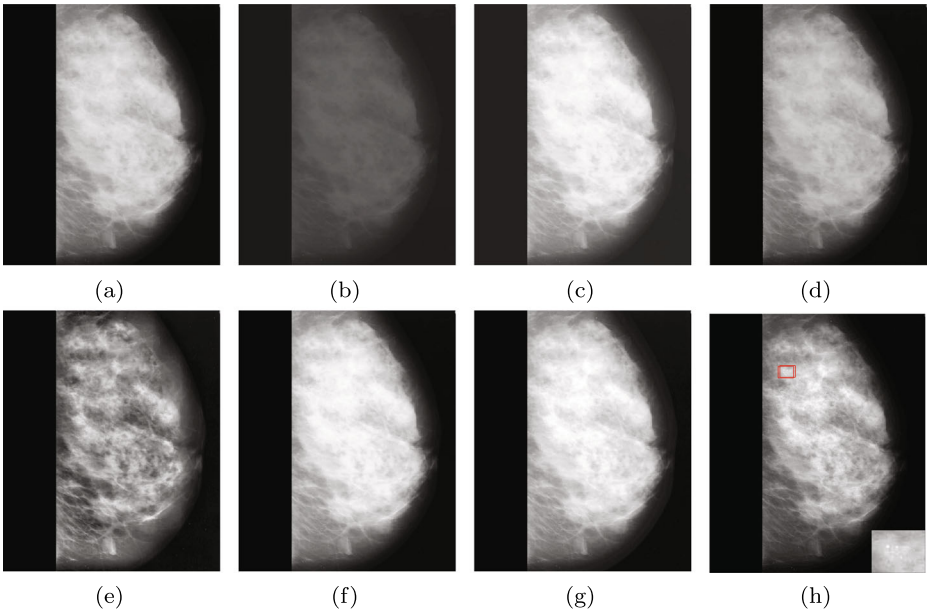

Fig. 5 Comparison of mammogram enhancement with different algorithms. (a) Original mammogram. Enhanced results by (b) RUM; (c) NSCUM; (d) AUM; (e) GUM; (f) MSR; (g) BPDFHE; (h) The proposed Bi-SCM. Note that RUM, NSCUM, AUM, and GUM are UM based methods; MSR is MD based method; BPDFHE is HE based method

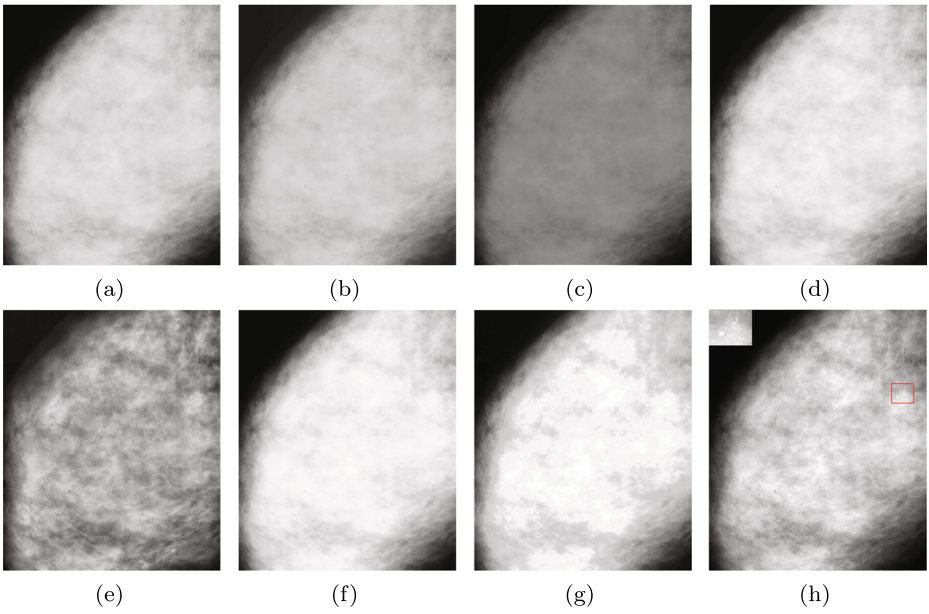

Fig. 6 Comparison of mammogram enhancement with different algorithms. (a) Original mammogram. Enhanced results by (b) RUM; (c) NSCUM; (d) AUM; (e) GUM; (f) MSR; (g) BPDFHE; (h) The proposed Bi-SCM. Note that RUM, NSCUM, AUM, and GUM are UM based methods; MSR is MD based method; BPDFHE is HE based method

Table 2 Initialized parameters for enhancement experiments

Algorithm	Parameters
RUM [36]	$\lambda = 2$
NSCUM [35]	$\lambda = 1$
GUM [12]	$\gamma_{\max} = 3, \gamma_{\min} = 1, \partial = 0.0005$
AUM [30]	$\tau_1 = 0.3,\ \tau_2 = 0.5,\ \alpha_h = 4,\ \alpha_l = 3$
	$\partial_b = 1,\ \mu = 0.1,\ \beta = 0.5$
MSR [34]	$c_1 = 20,\ c_2 = 80,\ c_3 = 200$
BPDFHE [38]	Parameters = [123454321]
Bi-SCM	$f = 0.02, g = 0.996, \lambda_{\max} = 3, \lambda_{\min} = 1, \gamma = 0.005$

The RUM, NSCUM and AUM are modified UM methods, which can enhance detail information. However, seeing Figs. 3(b)-6(b), Figs. 3(c)-6(c), and Figs. 3(d)-6(d), we can found that the contrast enhancement is almost indiscernible. Moreover, RUM introduces spot artifacts in enhanced images. GUM employs CLAHE [29] to enhance images, which produces over-enhancement in some portion of the image and enhances background noises, as shown in Figs. 3(e)-6(e). BPDFHE preserves the mean image-brightness, but introduces over-enhancement at the same time, leading to masses and micro-calcifications more undistinguishable than the original ones, as shown in Figs. 3(g)-6(g). In comparison with GUM and BPDFHE, the proposed Bi-SCM method can restrain noise amplification and over-enhancement to some extent. MSR simply takes reflectance as the final results, such that the light source directions of its enhanced images are confused, as shown in Figs. 3(f)-6(f). Comparing with MSR, the proposed Bi-SCM preserves the light source directions. In summary, one can see from the experimental results that the proposed Bi-SCM method not only improves the contrast but also enhances the details. In addition, it restrains noise amplification and over-enhancement. These observations indicate that the goal of the paper, which aims at enhancing visual quality of mammography images, is achieved by the proposed Bi-SCM.

To evaluate the quality of the enhanced mammography images quantitatively, the enhancement measures entitled measure of enhancement (EME) [1] and the increase of the number of visible edge (INVE) [18] are employed. EME is related to the ratio between the maximum intensity and the minimum intensity of a local region. Higher EME corresponds to more contrast improvement of the enhanced images. While INVE computes the ratio between the gradient of the visible edges before and after enhancement. Larger value of INVE indicates better enhancement performance of contrast and clearer visibility of details. Both of EME and INVE values greater than 2 indicate that contrast and detail visibility

Table 3 Quantitative measurement results of EME

Image	RUM	NSCUM	AUM	GUM	MSR	BPDFHE	Bi-SCM
Mam1	0.9322	1.9663	0.6410	3.0622	3.0963	2.4314	**3.3654**
Mam2	0.6700	0.9822	0.5381	1.6667	**4.3819**	1.2659	2.4955
Mam3	0.6424	0.6087	1.1835	2.3942	1.3386	1.5994	**3.9603**
Mam4	1.0481	2.6734	0.8125	2.4254	2.6014	2.4478	**3.1787**
Mam5	0.7791	1.1088	0.9627	1.6836	1.0551	1.5119	**2.0894**

Table 4 Quantitative measurement results of INVE

Image	RUM	NSCUM	AUM	GUM	MSR	BPDFHE	Bi-SCM
Mam1	-0.5691	1.0252	-0.9783	2.3532	1.9105	0.3445	**2.8158**
Mam2	-0.2993	0.1928	-0.8587	1.1004	1.1628	0.8306	**2.4237**
Mam3	-0.3832	-0.7491	0.4371	3.9919	1.5487	2.1209	**4.5953**
Mam4	-0.1312	2.6147	-0.8261	4.5374	2.2565	5.1088	**5.3424**
Mam5	0.6199	1.4954	1.0092	2.4121	1.4057	1.3212	**3.5310**

are well enhanced. The EME and INVE values of five mammograms are listed in Tables 3 and 4, respectively. And the best records are marked in bold. Examining Tables 3 and 4, we can conclude that the values of EME and INVE from GUM, MSR, and our UM scheme are higher than those of the rest algorithms, reflecting the state-of-the-art performance of the proposed Bi-SCM approach.

In order to report the overall results on 50 test mammograms, we plot box plots in terms of EME and INVE values in Figs. 7 and 8, respectively. One can conclude from Figs. 7 and 8 that the proposed Bi-SCM achieves better performance than state-of-the-art enhancement methods, while the GUM method takes the second place.

3.3 Discussions

The conventional SCM model makes full use of the intensity distribution and spatial information of image to improve contrast. When SCM is used to enhance images, bright areas would be processed more coarsely than dark areas, resulting in losing information of lesions. To overcome the drawbacks of SCM, we propose a Bi-SCM model to improve the contrast while avoiding information loss, making the lesions being highlighted from complex background. However, fusing the two SCM-enhanced results increases the computational complexity.

Specially, the proposed method is implemented by MATLAB R2010b on a PC with Intel i5 processer and 8 GB RAM. The average processing time for one test image with

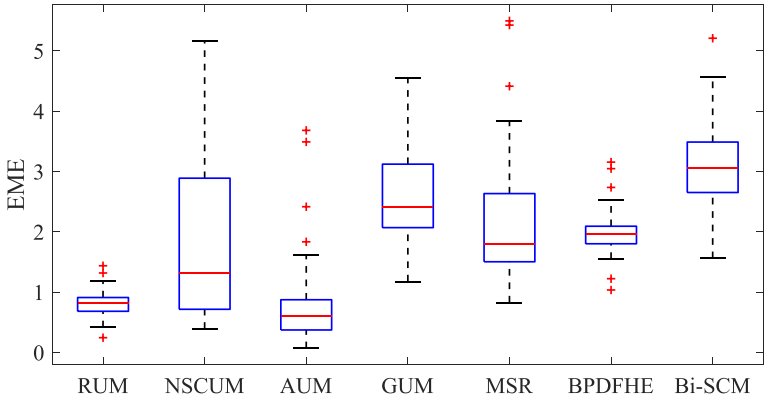

Fig. 7 Box-plots of EME for 50 test images

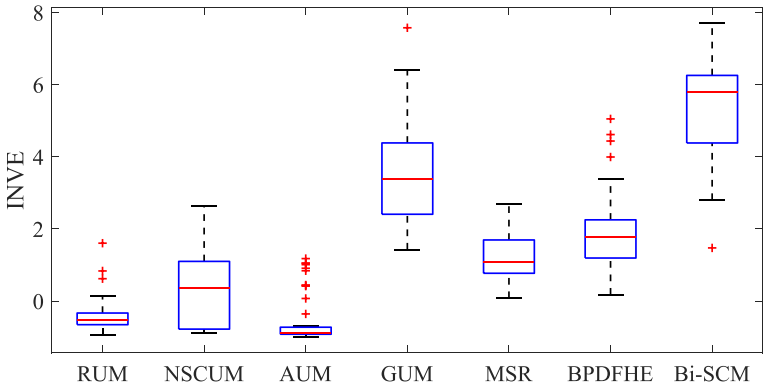

Fig. 8 Box-plots of INVE for 50 test images

256×256 pixels is 61.8774s. This is primary because the NSCT based fusion algorithm is a computationally intensive process. While the running time of SCM model is only 0.3293s. In the future, the efficiency of Bi-SCM can be improved from either implementation point-of-view or algorithm point-of-view. First, the Bi-SCM model is currently implemented by software for sequential processing on CPU, which heavily limits the processing speed of the algorithm. One important future research direction is to implement Bi-SCM by parallelly programming on multi-thread processors, such as GPU or FPGA. Second, a comprehensive study of different fusion algorithms will be conducted to reduce the computational burden of fusion process.

4 Conclusion

In this paper, a Bi-SCM model with unsharp masking is proposed for the purpose of enhancing both contrast and textural details of mammography images. The proposed Bi-SCM method not only explores the neural spiking ability in low-contrast image enhancement from a bidirectional way, but also is the first attempt which leverages neural spiking mechanism and unsharp masking to improve both both contrast and textural details. Sufficient experimental results on real breast mammography images show that the proposed method not only improves contrast and enhances details, but also reduces noise amplification and over-enhancement without the priori knowledge of image contents.

In addition, high-quality imaging is an important technique for early detection of tumors, which is further an important way to reduce the death rate caused by breast cancer among women. The proposed Bi-SCM is able to significantly improve the visual quality of mammography images that are usually limited by X-ray hardware systems. Therefore, the proposed method has high potential and shows clinical significance for radiologists to detect and diagnose breast cancer.

Acknowledgments This work was jointly supported by the National Natural Science Foundation of China under grant 62001110, the Natural Science Foundation of Jiangsu Province under grant BK20200353, andthe 111 Project under grant B17040.

Data Availability The datasets analysed during the current study are available at https://www.mammoimage.org/databases/ and http://www.eng.usf.edu/cvprg/Mammography/Database.html.

Declarations

Conflict of Interests The authors declare that they have no conflicts of interest.

References

1. Agaian SS, Panetta K, Grigoryan AM (2001) Transform-based image enhancement algorithms with performance measure. IEEE Trans Image Process 10(3):367–382
2. Bhatnagar G, Wu QMJ, Liu Z (2009) Directive contrast based multimodal medical image fusion in NSCT domain. IEEE Trans Multimedia 20(12):1980–1986
3. Celik T, Tjahjadi T (2012) Automatic image equalization and contrast enhancement using Gaussian mixture modeling. IEEE Trans Image Process 21(1):145–156
4. Chen S-D, Ramli A (2003) Minimum mean brightness error bi-histogram equalization in contrast enhancement. IEEE Trans. Consum Electron 49(4):1310–1319
5. Diwakar M, Kumar M (2018) A review on CT image noise and its denoising. Biomed Signal Process Control 42:73–88
6. Diwakar M, Kumar P (2019) Wavelet packet based CT image denoising using bilateral method and Bayes Shrinkage rule. In: Handbook of Multimedia Information Security, pp 501–511
7. Diwakar M, Kumar P (2020) Blind noise estimation-based CT image denoising in tetrolet domain. Int J Inf Comput Secur 12(2/3):234–252
8. Diwakar M, Kumar P, Singh AK (2020) CT Image denoising using NLM and its method noise thresholding. Multim Tools Appl 79(21-22):14449–14464
9. Diwakar M, Singh P (2020) CT Image denoising using multivariate model and its method noise thresholding in non-subsampled shearlet domain. Biomed Signal Process Control 571(57):101754
10. Diwakar M, Sonam M (2015) Kumar CT image denoising based on complex wavelet transform using local adaptive thresholding and Bilateral filtering. In: Proc Int Symposium on Women in Computing and Informatics, pp 297–302
11. Diwakar M, Verma A, Lamba S, Gupta H (2018) Inter- and Intra-scale Dependencies-Based CT Image Denoising in Curvelet Domain. In: Proc Soft Computing Theories and Applications. Advances in Intelligent Systems and Computing, pp 343–350
12. Deng G (2011) A generalized unsharp masking algorithm. IEEE Trans Image Process 20(5):1249–1261
13. Eckhorn R (1990) Feature linking via Synchro-nization among distributed assembles: simulations of results from cat visual cortex. Neural Comput 2:293–307
14. Eltoukhy MM, Faye I, Samir BB (2008) A comparison of wavelet and curvelet for breast cancer diagnosis in digital mammogram. Comput Biol Med 40(4):384–391
15. Fechner GT (1860) Elemente der psychophysik, 1st ed. Bre-itkopf & Hartel, Leipzig
16. Gao X, Wang Y, Li X, Tao D (2010) On combining morphological component analysis and concentric morphology model for mammographic mass detection. IEEE Trans Inf Technol Biomed 14(2):266–273
17. Ghita O, Ilea DE, Whelan PF (2013) Texture enhanced histogram equalization using TV $- l_1$ image decomposition. IEEE Trans Image Process 22(8):3133–3144
18. Hautière N, Tarel J-P, Aubert D, Dumont E (2011) Blind contrast restoration assessment by gradient rationing at visible edges. Image Anal Stereol 27(2):87–95
19. Heath M, Bowyer K, Kopans D, Moore R (2001) The digital database for screening mammography. In: Proc 5th Int Workshop Digital Mammography, pp 212–218
20. Hu K, Gao X, Li F (2011) Detection of suspicious lesions by adaptive thresholding based on multiresolution analysis in mammograms. IEEE Trans Instrum Meas 60(2):462–472
21. Jung S-W (2014) Image contrast enhancement using color and depth histograms. IEEE Signal Process Lett 21(4):382–385
22. Kim YT (1997) Contrast enhancement using brightness preserving bi-histogram equalization. IEEE Trans Consum Electron 43(1):1–8
23. Lakshmanan R, Thomas V (2012) Enhancement of microcalcification features using morphology and contourlet transform. In: Proc Int Conf advances in Comput and Commun Cochin, pp 14–17
24. Lu Z, Jiang T, Hu G, Wang X (2007) Contourlet based mammographic image enhancement. In: Proc Int Conf Photonics and Imaging in Biology and Medicine, Wuhan, pp 65340M-1-65340M-8
25. Ma Y, Teng F, Zhan K, Zhang H (2012) A new method of color image enhancement using spiking cortical model. Journal of Beijing University of Posts and Telecomminications (Chinese) 35(3):70–73

26. Mai C, Nguyen M, Kwok N (2011) A modified unsharp masking method using particle swarm optimization. In: Proc Int Cong Image and Signal Processing, Shanghai, pp 646–650
27. Panetta K, Zhou Y, Agaian S, Jia H (2011) Nonlinear unsharp masking for mammogram enhancement. IEEE T Inf Technol Biomed 15(6):918–928
28. Petrovic V (2007) Subjective tests for image fusion evaluation and objective metric validation. Inf Fusion 8(2):208–216
29. Pizer SM, Amburn EP, Austin JD, Cromartie R, Geselowitz A, Greer T, Romeny BTH, Zimmerman JB (1987) Adaptive histogram equalization and its variations. Comput Vis Graph 39(3):355–368
30. Polesel A, Ramponi G, Mathews VJ (2000) Image enhancement via adaptive unsharp masking. IEEE Trans Image Process 9(3):505–510
31. Qu G, Zhang D, Yan P (2001) Medical image fusion by wavelet transform modulus maxima. Opt Express 9(4):184–190
32. Qu G, Zhang D, Yan P (2002) Information measure for performance of image fusion. Electron Lett 38(7):313–315
33. Qu X, Yan J-W, Yang G-D (2009) Sum-modified-laplacian-based multifocus image fusion method in sharp frequency localized contourlet transform domain. Opt Precision Eng 17(5):1203–1212
34. Rahman Z, Jobson DJ, Woodell GA (1996) Multi-scale retinex for color image enhancement. In: Proc Int Conf Image Processing, Lausanne, pp 1003–1006
35. Ramponi G (1998) A cubic unsharp masking technique for contrast enhancement. Signal Process 67(2):212–222
36. Ramponi G, Polesel A (1998) Rational unsharp masking technique. J Electron Imag 7(2):333–338
37. Ranganath HS, Kuntimad G, Johnson JL (1995) Pulse coupled neural networks for image processing. In: Proc IEEE Southeastcon, Raleigh, NC, pp 37–43
38. Sheet D, Garud H, Suveer A, Mahadevappa M, Chatterjee J (2010) Brightness preserving dynamic fuzzy histogram equalization. IEEE Trans Consum Electron 56(4):2475–2480
39. Stewart DE, Cheung AM, Duff S, Wong F, McQuestion M, Cheng T, Purdy L, Bunston T (2001) Attributions of cause and recurrence in long-term breast cancer survivors. Psychooncology 10(2):179–183
40. Suckling J, Parker J, Astley S, Hutt I, Boggis C, Ricketts I, Stamatakis E, Cerneaz N, Sl K, Taylor P, Betal D, Savage J (1994) The mammographic image analysis society digital mammogram database. In: Proc 2nd Int Workshop Digital Mammography, pp 375–378
41. Sun X, Du J, Li Q, Li X (2013) Improved energy contrast image fusion based on nonsubsampled contourlet transform. In: Proc IEEE int conf industrial electronics and applications, Melbourne, VIC, pp 1610–1613
42. Toet A, Van Ruyven LJ, Valeton JM (1989) Merging themal and visual images by a contrast Pyramid. Opt Eng 28(7):789–792
43. Wang Z, Ma Y (2008) Medical image fusion using m-PCNN. Inf Fusion 9(2):176–185
44. Xing S-X, Chen T-H, Li J-X (2010) Image fusion based on regional energy and standard deviation. In: Proc Int Conf signal process Systems, Dalian, pp V1-739-V1-743
45. Xiao X, Zhang X (2010) An improved unsharp masking method for borehole image enhancement. In: Proc Int Conf Industrial Mechatronics and Automation, Wuhan, pp 349–352
46. Xydeas CS, Petrovic V (2000) Objective image fusion performance measure. Electron Lett 36(4):308–309
47. Zhan K, Zhang H, Ma Y (2009) New spiking cortical model for invariant texture retrieval and image processing. IEEE Trans Neural Netw 20(12):1980–1986